# CONFINEMENT AND EQUILIBRIUM WITH INTERNAL ISLANDS IN A CONFIGURATION SCAN WITH RESPECT TO IOTA IN W7-X

**J. GEIGER***, T. ANDREEVA, A. DINKLAGE, M. HIRSCH, H. THOMSEN, C. D. BEIDLER, M. BEURSKENS, S. BOZHENKOV, R. BRAKEL, C. BRANDT, K. J. BRUNNER, R. BURHENN, V. BYKOV, G. FUCHERT, M. GRAHL, O. GRULKE, U. HÖFEL, M. JAKUBOWSKI, T. KLINGER, J. KNAUER, A. LANGENBERG, S. LAZERSON, U. NEUNER, C. NÜHRENBERG, K. RAHBARNIA, J. SCHILLING, T. WINDISCH, J. ZHU
Max-Planck-Institute for Plasma Physics, Greifswald, Germany
*Email: joachim.geiger@ipp.mpg.de

Y. SUZUKI
National Institute for Fusion Science, Toki, Gifu, Japan

G. A. WURDEN
Los Alamos National Laboratory, Los Alamos, NM, USA

A. ALONSO
Laboratorio Nacional de Fusión, CIEMAT, Madrid, Spain

G. KOCSIS, M. VÉCSEI, S. ZOLETNIK
Centre for Energy Research, Budapest, Hungary

A. KRÄMER-FLECKEN
Institute of Climate and Energy Research – Plasma Physics, Forschungszentrum Jülich, Jülich, Germany

N. PABLANT
Princeton Plasma Physics Laboratory, Princeton, NJ, USA

J. C. SCHMITT
Auburn University, Auburn, AL, USA

E. TRIER
Max-Planck-Institute for Plasma Physics, Garching bei München, Germany

AND THE W7-X TEAM

**Abstract**

A dedicated scan of magnetic configurations in Wendelstein 7-X has been performed with respect to the rotational transform $\iota$ to investigate the confinement properties in configurations located between the major resonances providing boundary islands for proper island divertor operation. The scan investigated configurations between the so-called high-iota configuration with the 5/4-islands at the boundary and the so-called standard configuration with the 5/5-islands at the boundary. In particular, when the vacuum-$\iota$ of the configuration is reduced starting from high-iota, the resonance $\iota$=1 appears at the plasma centre and moves outward (as 5/5-island chain in the confinement region) due to the positive shear (in the stellarator sense, $d\iota/dr>0$) of the vacuum $\iota$-profiles in W7-X. For the main part of the scan, the 5/5-island chain was located in the outer third of the plasma with respect to the minor radius. The experimental conditions had been chosen at a line-integrated density of $3.5 \cdot 10^{19} m^{-2}$ and an ECRH power of 2MW (140GHz, X2). The paper summarizes the main observations that the plasma energy measured by the diamagnetic coils increases with decreasing vacuum-$\iota$ while the observed MHD-activity, which is connected to the outward moving 5/5-islands, increases in strength. The increase in plasma energy is attributed to an increase in confinement since it persists even if one accounts for volume changes due to the changes in configurations. The paper also presents MHD-equilibrium calculations using the HINT-code, which can treat islands in the confinement region properly, and compares them with the results of the VMEC-code which by itself cannot treat this situation since it is based on the assumption of nested flux surfaces. However, in combination with the EXTENDER-code, an approximation of the equilibrium field with islands can be provided. The differences in the results of these approaches are discussed.

## 1. INTRODUCTION

Wendelstein 7-X (W7-X) is an advanced stellarator [1] designed to explore the reactor viability of optimized stellarators. An optimization procedure for the magnetic configuration targeted the MHD-equilibrium and -stability properties (β-limit in the range of volume-averaged ‹β›-values of about 5%), low neoclassical transport and small bootstrap current in the long-mean-free-path regime, and good fast-particle confinement at sufficiently high β-values. The result was a 5-period configuration with a toroidal mirror field of about 10%, i.e. a variation of the field strength along the magnetic axis of ±10%, with a major radius of 5.5m and a minor radius of about 0.5m. To explore long-pulse operation, the optimized configuration has been realized with a superconducting coil system consisting of 50 non-planar coils (NPC) (10 per period) and 20 planar coils (PC) (4 per period). One period of the coil system is shown in Fig. 1. Stellarator-symmetry reduces the number of coil types by a factor of 2, i.e. there are 5 NPC and 2 PC types as indicated by the numbering in Fig.1. Each coil type has an independent power supply allowing for a high flexibility in choosing magnetic configurations. The NPCs provide a base configuration with equal coil currents, the so-called standard reference configuration, having a boundary rotational transform $\iota_b$ of 1, which leads to the appearance of a 5/5-island chain which can be used for island divertor operation. Adjusting the coil currents in the different NPCs changes the variation of the field strength toroidally from almost constant along the axis to a variation of about ±10%, at which the optimized configuration is attained. The PC are used to vary the vacuum-$\iota$ of the configuration by using equal currents in the PCs, but also to introduce an inward- or outward-shift of the plasma by unequal current feeding of the PCs due to the mutual inclination of coil types A and B (see Fig.1). Two additional normal-conducting coil systems enlarge the experimental flexibility. First, 10 control coils (CCs) (2 per period, stellarator-symmetric) shown in Fig.1 allow the size and phase of the boundary islands to be changed, each CC having its own power supply. Second, a set of 5 trim coils can be used to compensate and/or study error fields in W7-X.

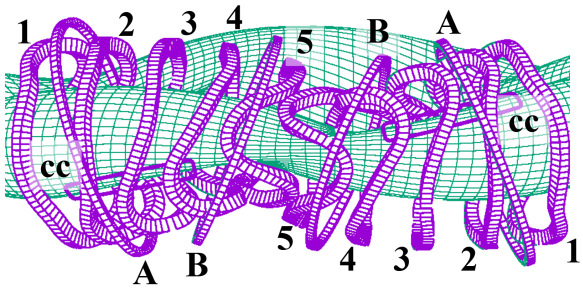


*Fig. 1: One period of the coil system of W7-X with the non-planar coils numbered from 1 to 5, the planar coils A and B, and the paper-clip-like control coils marked with "cc".*

The device started operation in December 2015 with a simple uncooled limiter for an integral commissioning phase of about three months. In 2016/17 an uncooled divertor, the so-called test-divertor-unit (TDU), was installed which has the same geometry as the water-cooled high-heat-flux (HHF) divertor (currently undergoing installation). Two campaigns, lasting about 3 months each in 2017 and 2018, were performed for a first exploration of divertor plasmas [2], for initial testing of the optimization goals in various magnetic configurations, as far as plasma parameters allowed, and for addressing a wider range of physics questions like heating schemes, current drive or turbulence investigations.

One physics topic which is of great interest for stellarators, in particular low-shear stellarators such as W7-X, is the impact of the rotational transform on the configuration properties. Besides the effect that higher $\iota$ is preferable to reduce the Shafranov-shift and to allow higher values of the equilibrium-β-limit, there is also the observation that confinement can change notably in low-shear configurations when $\iota$ is adjusted. The appearance of rational values of $\iota$ within the plasma can destabilize MHD-modes, but has also been observed to be important in connection with internal transport barriers. In particular, it is known that rational values of $\iota$ appearing at the edge can lead to changes in the confinement behaviour of magnetic configurations, examples being the appearance of the so-called $\iota$-windows of the H-mode in devices like W7-AS [3] or Heliotron-J [4]. Therefore, a dedicated scan of $\iota$ was performed in 2018 to investigate this effect on confinement, equilibrium and stability in W7-X. The latter is of interest because low-order rationals appear inside the confinement region. A particular difficulty for such experiments is the calculation of the proper MHD-equilibrium. For stellarators, the 3D-MHD-equilibrium code VMEC [5] is used world-wide as the work-horse for this task. However, VMEC's numerical scheme assumes that the equilibrium consists of nested flux surfaces and therefore cannot treat fields with islands in the confinement region properly. If VMEC is nevertheless employed, it produces a magnetic field with nested flux surfaces without islands. The HINT-code [6,7] was developed to calculate fields with islands and regions with chaotic field lines. It solves resistive MHD-equations on a spatial grid as an initial-value problem in such a way that steady-state force balance is eventually realized. With HINT, it is thus possible to investigate the effect of islands consistently in the MHD-equilibrium. It is also possible to make the islands visible using a VMEC-calculation via a recalculation of the magnetic field by combining the vacuum field from coils with the plasma generated field calculated from VMEC using the EXTENDER code [8,9,10]. This

approach, however, does not generate a consistent MHD-equilibrium field since the plasma-generated fields are based on a nested-flux-surface equilibrium, ignoring deformations of the equilibrium currents due to the islands.

The paper summarizes the experiments and their results [11,12] in terms of the experimental observations. The calculations using HINT are then presented together with results of VMEC-calculations and of the VMEC/EXTENDER-approach which are compared and discussed.

## 2. EXPERIMENTS AND RESULTS

The vacuum-$\iota$ has been varied between a configuration with the 5/5-islands at the boundary ($\iota_b$ =1) as lower bound (so-called standard configuration) while the upper bound is given by the so-called High-iota configuration ($\iota_b$ =5/4) with the 5/4-island chain forming the plasma boundary. Both configurations are island divertor configurations since the islands and their separatrix interacts with the divertor for particle and energy exhaust. The configurations in-between these two boundaries are limiter configurations, i.e. nested flux surfaces intersect the divertor. One should note that for some configurations higher-order rationals appear at the boundary with the corresponding island structures, e.g. the 10/9-islands, but these have smaller island widths. Nevertheless, such structures can play a role in confinement changes, too. Table 1 summarizes the magnetic configurations of the scan [11] in terms of the experiment-ID and the internal naming of the configurations (W7-X-spec., the "+252" marks the field strength on axis in the ECRH launching plane in units of 10mT) with the coil currents of the NPCs and PCs and the ι-values at the centre and the boundary. For easier referencing the configurations/experiments are named with a letter (***A*** to ***Q***) sequentially following the order of the experiment IDs. The current in the CCs is also provided as the CCs have been used in island-width-variation experiments in one configuration, i.e. experiments ***I*** and ***N*** are the same configuration in terms of the coil currents.

TABLE 1. EXPERIMENTS IN IOTA-SCAN: NAMING AND VACUUM FIELD PROPERTIES

| name | exp. ID | W7-X-spec. | NPC-curr. [A] | PC-curr. [A] | CC curr. [A] | $\iota_0$ | $\iota_b$ |
|---|---|---|---|---|---|---|---|
| ***A*** | 20180927.09 | FTM001+252 | 14219 | -10040 | 0 | 1.012 | 1.210 |
| ***B*** | 20180927.15 | FQM001+252 | 13883 | -7290 | 0 | 0.965 | 1.167 |
| ***C*** | 20180927.16 | FOM003+252 | 13608 | -5040 | 0 | 0.928 | 1.099 |
| ***D*** | 20180927.17 | FNM+252 | 13577 | -4790 | 0 | 0.924 | 1.094 |
| ***E*** | 20180927.18 | FNM001+252 | 13546 | -4540 | 0 | 0.920 | 1.089 |
| ***F*** | 20180927.19 | FNM002+252 | 13515 | -4290 | 0 | 0.916 | 1.084 |
| ***G*** | 20180927.20 | FMM+252 | 13485 | -4040 | 0 | 0.912 | 1.078 |
| ***H*** | 20180927.21 | FMM001+252 | 13454 | -3790 | 0 | 0.908 | 1.069 |
| ***I*** | 20180927.22 | FMM002+252 | 13423 | -3540 | 0 | 0.904 | 1.066 |
| ***J*** | 20180927.28 | FMM003+252 | 13392 | -3290 | 0 | 0.900 | 1.061 |
| ***K*** | 20180927.29 | FLM+252 | 13361 | -3040 | 0 | 0.897 | 1.054 |
| ***L*** | 20180927.30 | EJM+252 | 13114 | -1040 | 0 | 0.862 | 0.984 |
| ***M*** | 20180927.33 | EJM004+252 | 13016 | -250 | 0 | 0.854 | 0.984 |
| | | | | | | | |
| ***N*** | 20181017.21 | FMM002+252 | 13423 | -3540 | 0 | 0.904 | 1.066 |
| ***O*** | 20181017.22 | FMM002+252 | 13423 | -3540 | -1745 | 0.904 | 1.066 |
| ***P*** | 20181017.23 | FMM002+252 | 13423 | -3540 | -1000 | 0.904 | 1.066 |
| ***Q*** | 20181017.24 | FMM002+252 | 13423 | -3540 | +1000 | 0.904 | 1.066 |

Fig. 2 shows the Poincaré-plots of four configurations of the scan, the one with the lowest vacuum-$\iota$, i.e. a standard-configuration type with the 5/5-islands at a proper island divertor position and the one with the highest vacuum-$\iota$ with the 5/4-islands forming the plasma boundary, also at a proper island divertor position. The two intermediate ones show the locations of the 5/5-islands in the scan and configuration ***I*** exemplifies how close the islands are to the divertor at the low-$\iota$ end of the scan. The experiments of the scan were generally performed in discharges with 4 seconds at 2MW ECRH-power (140GHz, X2-mode) and a line density of $3.5 \cdot 10^{19} m^{-2}$. Fig. 3 shows typical time traces for heating power, line density from interferometry and diamagnetic energy. In

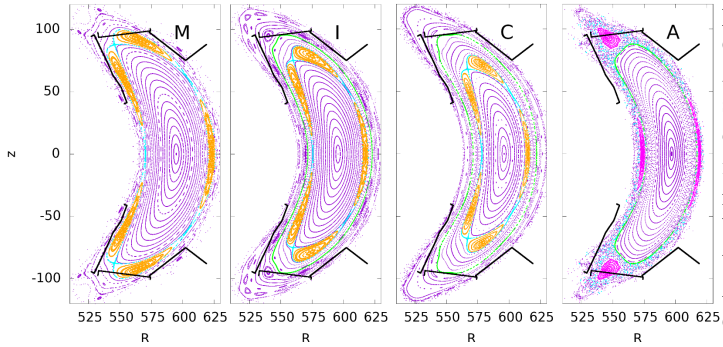


Fig. 2: Poincaré-plots of configurations of the scan in order of increasing vacuum-$\iota$. The 5/5-islands are marked with orange, the separatrix with cyan and the lmsf with green. Left to right: Standard configuration (***M***) with 5/5-islands intersecting the divertor, intermediate limiter configurations ***I*** and ***C*** in which the 5/5-islands move inward due to increasing vacuum-$\iota$ and positive shear, and high-iota configuration (***A***) with 5/4-islands marked in magenta.

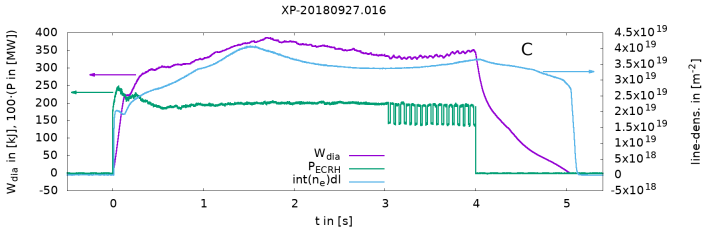


Fig. 3: Time traces of ECRH-power (green), line-integrated electron density from interferometry and diamagnetic energy for discharge XP-20180927.16 corresponding to configuration/experiment-name ***C***.

particular, the power scenario generally contained power modulation (17Hz, $\Delta P$=600kW) for heat wave studies in the last second. The effect of the power modulation on the energy content was marginal as seen in Fig. 3. Note also that the line density was not perfectly constant during the discharges but most of the line density traces met the target density around the time of 3.5s. Additional deviations from the general discharge scenario are to be noted for the discharges ***A*** and ***M*** which ran for almost 30s and 26s, respectively, with power modulation in the last 4 and 2 seconds, respectively. In the time range of up to 4 seconds, the plasma current in all discharges stayed below 1kA, except for the standard configuration type cases ***L*** and ***M*** but even for those the plasma current was still below 2.5kA and can therefore be neglected. An estimation of the effect of 1kA plasma current with a simple cylindrical approximation results in $\Delta\iota\approx0.0017$ for a minor radius of 0.5m, a major radius of 5.5m and a field strength of 2.5T. Finally, the island-variation experiments ***N*** to ***Q***, performed on a different day, have been run with a line-density of about $6\cdot10^{19}$m$^{-2}$.

Fig. 4 (right) compares the achieved diamagnetic energies (purple bullets) achieved in the different magnetic configurations. It is notable that the energies increase as $\iota$ is lowered starting from configuration ***A*** to configurations ***J*** and ***K*** and are again smaller for the standard configuration types ***L*** and ***M***. One part in this energy change may be caused by a change in the volume of the nested-flux-surface region available for the plasma which is shown in Fig. 4 (left) as red bullets. Additional configurations not run in the scan are also shown to provide a more complete picture. The main reasons for the volume changes at the boundaries of the scan are due to switching from a separatrix configuration (volume without boundary islands) to a limiter configuration (bigger islands inside) as can be seen in Fig. 4 (left). There is additionally an effect on the volume because the flux surfaces become less vertically elongated when the vacuum-$\iota$-value is reduced. This leads to the moderate increase in volume for the configurations from ***B*** to ***K*** as $\iota$ is lowered. In Fig. 4 (right) this volume effect is accounted for by scaling the diamagnetic energies to a specific volume of 31.5m$^3$ for all configurations for better comparison. This lifts the points of the separatrix configurations notably, but for the finer scan the results are less affected. Density has also an effect on confinement seen in scaling laws like ISS04 [13]. In particular, the line density for the two maximum energy configurations ***J*** and ***K*** in Fig. 4 had higher line density values making their top-position in the achieved energies questionable. Because for W7-X there are not yet conclusive results on the density dependence of the confinement time, i.e. $\tau_E\sim n_e^{\alpha}$, the effect is illustrated using a certain range of exponents $\alpha$ for a scaling-law-type density dependence. A

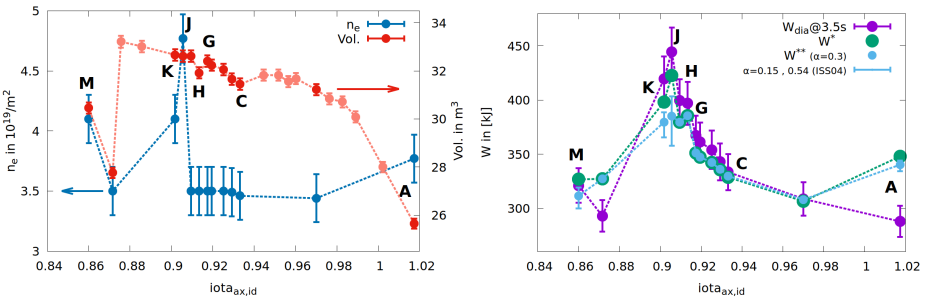


Fig. 4: Left: Line densities (blue, left y-axis) at 3.5s in scan and volumes of the vacuum magnetic configurations (red, right y-axis) vs the central $\iota$-value of the scan. Additional light-red points to show the general trend (not run in iota-scan). Right: diamagnetic energy (purple) at 3.5s. Green: Energies scaled to the same volume of 31.5m$^3$, i.e. $W^*=W_{dia}\cdot(31.5m^3/Vol(X))$. Light-blue: additional scaling to the same line density of $3.5\cdot10^{19}$m$^{-2}$ according to $W^{**}=W^*\cdot(3.5/n_e)^{\alpha}$ ($n_e$ in units of $10^{19}$m$^{-2}$). The bullets for $\alpha$=0.3 (moderate dependence), "error bars" show extent of a weak ($\alpha$=0.15) to a stronger ($\alpha$=0.54 from ISS04) density dependence.

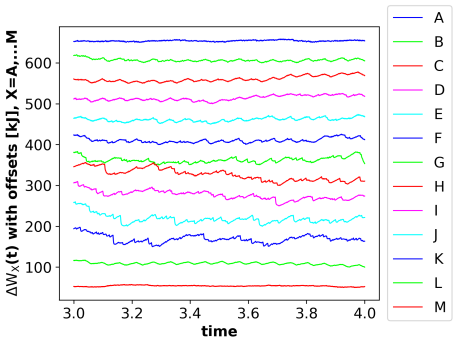


Fig. 5: Time traces of diamagn. energy with offsets for better distinction ordered by $\iota$. Top: high-iota. Bottom: standard config..

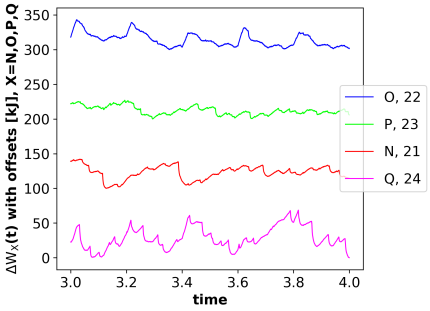


Fig. 6: Diamagn. energies in island width variation with offsets ordered by island size. Top trace: small island width. Bottom trace: enlarged island.

stronger $n_e$-dependence is provided by α from the ISS04-scaling (0.54), a moderate density dependence is simulated with a value of 0.3 and a weak dependence by α=0.15. The latter two values are currently somewhat arbitrary and serve to illustrate a certain range. The influence of the density scaling is treated like the volume effect by scaling the volume-scaled energies to the same line density value of $3.5 \cdot 10^{19} m^{-2}$. In Fig. 4 (right) the light-blue bullets represent the moderate density dependence while stronger and weaker dependence are illustrate by "error-bars". By a moderate density dependence, the peak-characteristic of the configurations ***J*** and ***K*** is removed and they build a broader range of configurations ***H*** to ***K*** with a notably increased confinement. In particular, since the density was kept at the same level from ***A*** to ***I***, the increase of the diamagnetic energy from ***G*** to ***H*** is unaffected by a global density dependence of the confinement. In connection to the improvement of the confinement with lowering the vacuum-$\iota$ and the movement of the 5/5-islands towards the plasma boundary, there is a notable increase in the MHD-activity which is observed in the fluctuation diagnostics (Mirnov, ECE, soft-X-ray camera system) but also in the equilibrium diagnostics (diamagnetic signal) and in the Rogowski-coil signal measuring the plasma current [11,12]. In particular, the MHD-activity is located at the islands [12] and has, accordingly, been referred to as ILMs ("Island-Localized-Modes"). Fig. 5 illustrates the level of MHD-activity by its effect on the diamagnetic energy signal in the range from 3s to 4s. Experiment ***A*** and ***M*** are quiet and because they are long discharges, there is also no power modulation during this time, which is seen in experiments ***B*** to ***E*** and in ***L***. Additionally to the power modulation on the energy signal there is a gradual increase of crashes due to ILM events from configuration ***E*** onwards, and in configuration ***G*** to ***K*** the crashes dominate and the power modulation is no longer visible to the eye. The strength of the MHD-activity is not only connected to the 5/5-island position but also depends on the width of the islands, which has been demonstrated in separate island-width-variation experiments using configuration ***I***. Fig. 6 shows the behaviour of the diamagnetic energy signals in a configuration variation using the control coils to vary the island size: strong decrease for experiment ***O***, moderate decrease for ***P***, standard island size for ***N***, and enlarged island size for ***Q***. The signal for ***O*** is very quiet and shows mainly the effect of 20ms-NBI-blips every 200ms, which were also present in ***Q***. The signals show a clear increase in MHD-activity correlated with the increase in island size from ***O*** to ***Q***. In experiment ***Q*** the NBI-blips are almost totally hidden in the MHD-activity. Note that crashes are also present in experiment ***O*** but are fairly small. Also, similar crashes are observed when the 5/4- or the 5/6-island chain is present in the outer regions of the plasma, the latter concerning so-called low-iota configurations which are not included here.

## 3. MHD-EQUILIBRIUM CALCULATIONS

MHD-equilibrium calculations for 3D-geometries generally use the VMEC-code. However, VMEC rests on the assumption that the equilibrium consists of nested flux surfaces. Thus islands or stochastic regions in the confinement region are excluded. With the so-called VMEC/EXTENDER-approach (VMEX) this shortcoming can be addressed in an approximate way. The vacuum field is in this case combined with plasma-generated fields extracted from a VMEC-calculation together with an EXTENDER-calculation. These fields can show changes in the confinement volume due to variations in the boundary island locations or width, but also internal islands can emerge. However, since the plasma-generated fields are based on VMEC-calculations, these fields are not true MHD-equilibrium fields because they do not include the plasma response to the changed magnetic topology, either internally or at the boundary. Consistent inclusion of the plasma response can be important, in particular when helical deformations in the plasma current densities coincide with topological structures generating them, for example internal islands. A consistent treatment of such effects is the strength of the HINT-code which can treat islands and stochastic regions in MHD-equilibria (amongst other codes like PIES, SIESTA and SPEC).

Calculations were performed for configurations ***B***, ***C***, ***H***, ***I***, ***J*** and ***K*** with a pressure profile $\sim(1\text{-}s)^2$ (peaking factor ($=\beta_0/\langle\beta\rangle$) of about 3, no pressure gradients at plasma boundary), where s is the normalized toroidal flux

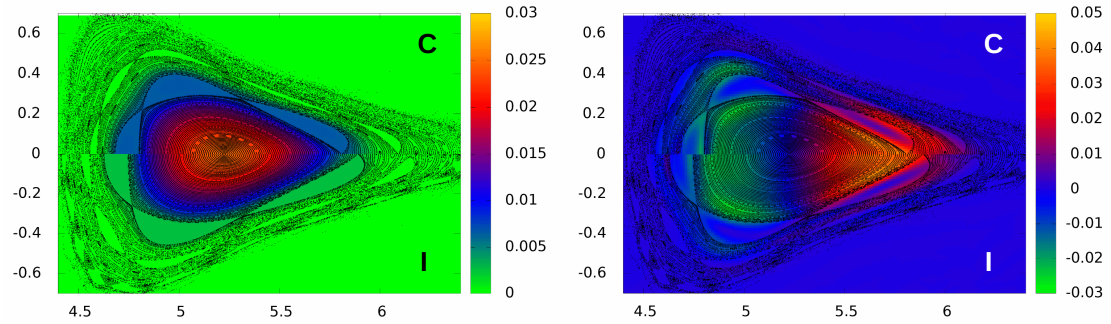


Fig. 7: Poincaré plots with underlying colour contours of pressure (left) and toroidal current density (right) of configurations ***C*** (upper half) and ***I*** (lower half).

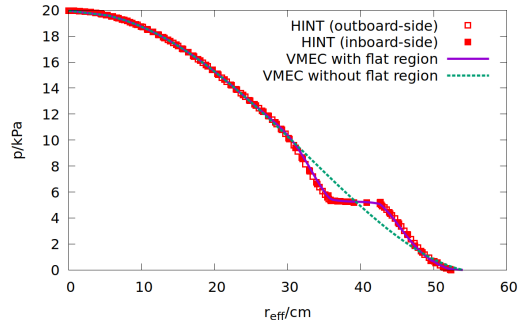


Fig. 8: Pressure profiles of HINT (red squares) and of two VMEC-calculations reproducing HINT's energy content, one accounting for the flattening due to the island (purple solid line), one ignoring it (green dashed line).

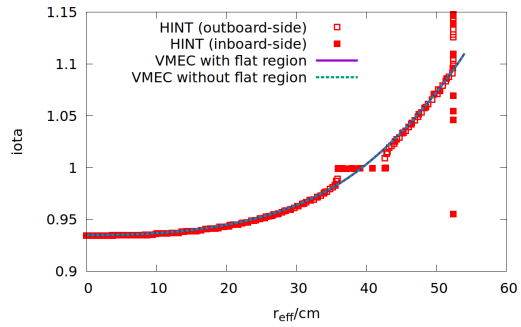


Fig. 9: Profiles of $\iota$ for HINT-calculation (red squares) and for two VMEC-calculations (purple solid line, green dashed line) shown in Fig. 8.

used as flux surface coordinate. Fig. 7 shows Poincaré-plots superimposed on colour contours of pressure and toroidal current density from calculations with central $\beta_0$=1% for configurations ***C*** and ***I***. The pressure contours show a constant pressure in the islands as would be expected from transport considerations (no heat or particle sources inside the islands) and accordingly the colour contours in the toroidal current density plot shows a depletion in the current density in the island regions (blue). Also clearly visible is the dipole structure of the Pfirsch-Schlüter-currents with negative (greenish) current density on the inboard side and positive (reddish) on the outboard side separated by blue (vanishing current density) passing through the magnetic axis.

The HINT-results have been compared to VMEC and to results of the VMEX-approach. Here, configuration ***C*** is used. For the comparison the final pressure profile of HINT has been mapped to the same minor radius as used in VMEC. Fig. 8 shows the pressure profiles of the HINT-calculation ($\beta_0$=1%) and two VMEC-calculations (purple and green lines). The former exhibits a flat region due to the island and increased gradients adjacent to this region, whereas the latter is characterised by similar gradients across this region but both profiles have the same total energy. In the $\iota$-profiles, the HINT-calculation has a similar flattening across the island, which is absent in both VMEC cases.

A direct comparison of the magnetic field topology is shown in Fig. 10 for the so-called triangular plane (phi=36°) at the half-period location. First, there is good agreement in the flux surfaces and the axis position of the different calculations. The VMEC flux surfaces penetrate the island structures present in the HINT-calculation and the VMEX-field as expected. This is the case for the 5/5-islands inside the confinement region, but also for the 10/9-islands at the plasma boundary. Although the 10/9-island chain in the HINT-field at the boundary is rather well reproduced with the VMEX-field, the 5/5-island chain in the VMEX-field is much smaller than the islands seen in the HINT-field. However, this effect is already seen when comparing a VMEX-field from a recalculation of the vacuum-field with the Biot-Savart-field. This deviation in island size shows the deficiency in the VMEX-approach in connection with internal islands. However, in case of the VMEC-field itself no islands appear at all.

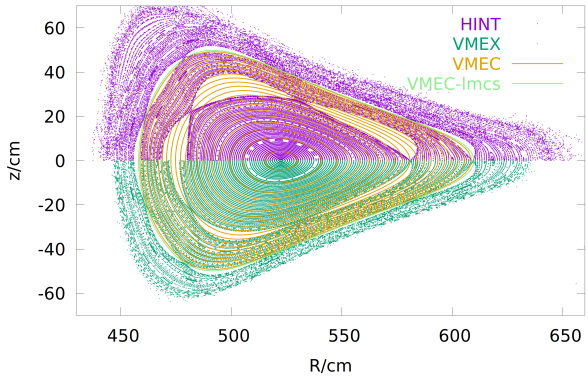


Fig. 10: Poincaré plots in the φ=36°-plane (triangular plane) for HINT (purple dots) and for the VMEX-field (green dots). Some VMEC flux surfaces are shown, too, in orange colour with the VMEC-boundary marked in light-green.

Fig. 11 exemplifies the effect of increasing β. The magnetic axis as well as the entire plasma is shifted

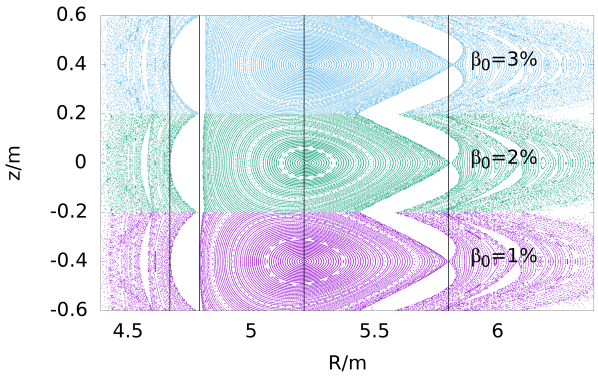


Fig. 11: Cutout of Poincaré plots for HINT-calculations of configuration ***C*** with central β-values of 1%, 2% and 3% (from bottom to top). The dashed lines serve to guide the eye to see the shifts of the axis and the outer x-point and also the increase in the island size on the inboard side island.

outward (→ Shafranov-shift) and the size of the 5/5-islands increases. To emphasize this, vertical lines have been added to guide the eye. Note that the 10/9-island shrinks. The β-values used in these calculations are in the range of the experimentally observed ones. $\beta_0$=1% corresponds to a plasma energy of about 350kJ for the field strength of the experiments. However, even with a peaking factor of 3, the volume-averaged β-values are much smaller than those envisioned for reactor-relevant W7-X operation, which is in the range of 4% to 5%.

The experimental observation of increasing MHD-activity in the iota-scan when the vacuum-$\iota$ is lowered is attributed to the radial outward movement of the 5/5-islands by which also the island width increases. This observation is complemented by the variation of the size of the 5/5-islands using the control coils in experiments ***N*** to ***Q***, where the configuration used in ***N*** is the same as in ***I***. Fig. 12 shows the Poincaré-plots of four HINT-calculations with $\beta_0$=1% in the four different configurations in one picture. The configurations are ordered by island size which starts with configuration ***Q*** with the increased island size in the lower left quadrant and moves clockwise via standard island size (***N***) to the configurations with decreased island size (***P*** and ***O***). Because of the relatively low β-values, the magnetic field structure still reflects much of the vacuum field. It is clearly seen that the increased 5/5-island move closer to the last closed magnetic surface (marked in black in Fig. 12) defined by the divertor components. MHD-activity arising from around the 5/5-islands is therefore closer to this boundary and, in case the energy in the islands is lost by this activity, the increased island volume leads to a stronger effect in the energy signals. The pressure profiles resulting in the HINT-calculations from an initial profile form ~$(1\text{-}s)^2$ are shown in Fig.13 along the major radius (z=0) in the triangular plane (same as in Fig. 12) and is complemented by the $\iota$-profile in fig. 14 along the same line. The effect of the island on the pressure flattening is clearly seen on the inboard side where the o-point is crossed and is not seen at the outboard side where the line crosses the x-point. Apart from the effect on the size of the 5/5-islands, it is notable that the configuration without control coils (***N***) has the best flux surface structure around and outside the 10/9-islands. The control coils seem to ergodize the region outside the 10/9-islands by causing high-order islands to overlap, whether the 5/5-island size is increased or decreased. It also seems that the decrease in 5/5-island size leads to an ergodization of the region around the 10/9-islands most visible in configuration ***O***. However, these effects are outside the last closed magnetic surface defined by the divertor components. Nevertheless, it should be noted that the stronger suppression of the 5/5-islands in configuration ***O*** leads to some ergodization around the 10/9-islands. Thus, stronger suppression of the 5/5-islands will lead to a higher degree of ergodization which can be seen in vacuum field calculations. Increasing β will also increase the island width as illustrated in Fig. 11. Note that the spatial gradients of the pressure do vary significantly close to the 5/5-

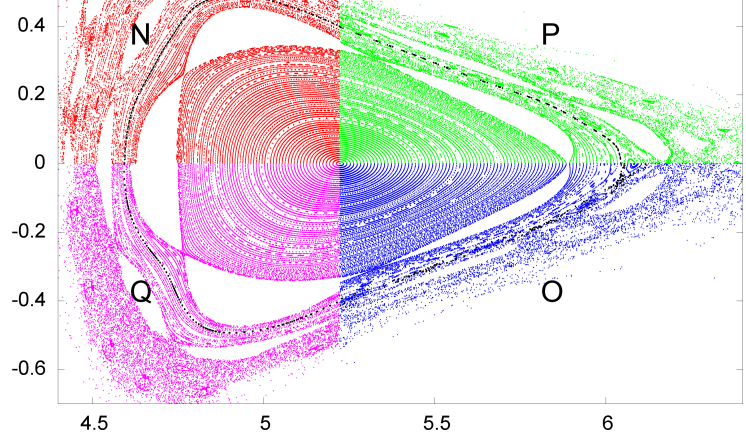


Fig. 12: Combination of Poincaré plots (φ=36°) of HINT-calculations with $\beta_0$=1% for the configurations varying the island width using the control coils, each differently coloured quarter belonging to the indicated configuration. The location of the last closed magnetic surface is indicated in black.

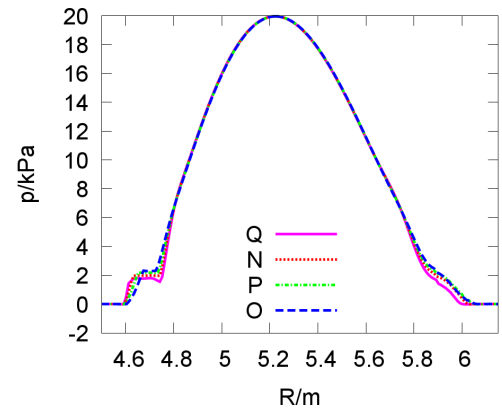


Fig. 13: Pressure profile of the HINT-calculations shown in Fig.12 in the φ=36°-plane along the R-axis. Same colour-coding as in Fig.12.

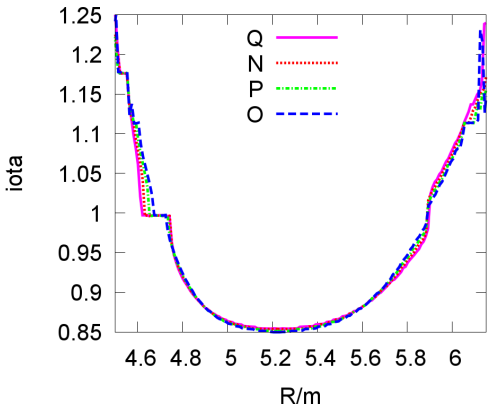


Fig. 14: Rotational transform profile of the HINT-calculations shown in Fig.12 in the φ=36°-plane along the R-axis. Same colour-coding as in Fig. 12.

island separatrix because of the flux surface deformations in the presence of the islands. This might be relevant for the excitation of the observed MHD-activity.

## 4. SUMMARY

An increase in confinement was observed in an iota-scan performed in W7-X between the high-iota and the standard configuration with decreasing value of the vacuum-$\iota$. The best confinement was achieved in configurations with the 5/5-island close to the plasma boundary. The improvement in confinement is about 15%. The increase in confinement is accompanied by an increase in MHD-activity related to the 5/5-islands location which grows as the islands move closer to the plasma boundary. The MHD-activity also grows with the island size which has been tested in experiments using the control coils to enlarge or reduce the island size.

MHD-equilibria for the configurations of the scan have been calculated using the HINT-code, which can treat islands in the confinement region, and the results have been compared with the VMEX-approach (VMEC/EXTENDER) which is faster but does not result in consistent MHD-equilibrium fields. It is found that the size of the internal islands are not well reproduced by the VMEX-approach. However, the overall agreement of the two results in terms of shift of the magnetic axis and the boundary fields is good. The internal 5/5-islands grow with β. For the configurations leading to the largest stored energy, the HINT-calculations show that the islands are rather close to the flux surfaces which are intersected by the divertor components. Moreover, the configurations varying the 5/5-island size using the control coils have been investigated, showing the effects of the different island sizes in the plasma profiles of the HINT-calculations. The impact of the control coils on the boundary magnetic field topology is seen to lead to ergodization around and outside of the 10/9-islands irrespective of whether the 5/5-islands are increased or decreased.

## ACKNOWLEDGEMENTS

This work has been carried out within the framework of the EUROfusion Consortium and has received funding from the Euratom research and training programme 2014-2018 and 2019-2020 under grant agreement No 633053. The views and opinions expressed herein do not necessarily reflect those of the European Commission. US researchers are supported by the US Dept. of Energy, Office of Fusion Energy Sciences.

## REFERENCES

[1] G. GRIEGER et al., Physics of Fluids B: Plasma Physics, 1992, 4, 2081-2091
[2] R. WOLF et al., Physics of Plasmas, 2019, 26, 082504
[3] M. HIRSCH et al., Plasma Phys. Control. Fusion, 2008, 50, 053001 (specifically chapter 7.4)
[4] F. SANO et al., Fusion Science and Techn., 2004, 46, 288-298
[5] S. HIRSHMAN et al., Comput. Phys. Comm., 1986, 43, 143-155
[6] K. HARAFUJI et al., J. Comput. Phys., 1989, 81, 169-192
[7] Y. SUZUKI et al., Nucl. Fusion, 2006, 46, L19-L24
[8] M. DREVLAK et al., Nucl. Fusion, 2005, 45, 731-740
[9] J. GEIGER et al., Contrib. Plasma Phys., 2010, 50, 770-774
[10] J. GEIGER et al., Contrib. Plasma Phys., 2011, 51, 99-99
[11] T. ANDREEVA, et al., in Proceedings of 46th EPS Conference on Plasma Physics, Milan (Italy), 8.-12.07.2019. http://ocs.ciemat.es/EPS2019PAP/pdf/P2.1063.pdf
[12] G. A. WURDEN, et al., in Proceedings of 46th EPS Conference on Plasma Physics, Milan (Italy), 8.-12.07.2019. http://ocs.ciemat.es/EPS2019PAP/pdf/P2.1068.pdf
[13] H. YAMADA et al., Nucl. Fusion, 2005, 45, 1684-1693